THE JOURNAL OF BIOLOGICAL CHEMISTRY VOL. 285, NO. 34, pp. 26315–26325, August 20, 2010

Identification of a Substrate-binding Site in a Peroxisomal β-Oxidation Enzyme by Photoaffinity Labeling with a Novel Palmitoyl Derivative*[S]

Received for publication, January 15, 2010, and in revised form, May 28, 2010 Published, JBC Papers in Press, June 21, 2010, DOI 10.1074/jbc.M110.104547

Yoshinori Kashiwayama[‡1], Takenori Tomohiro[§1], Kotomi Narita[‡], Miyuki Suzumura[§], Tuomo Glumoff[¶], J. Kalervo Hiltunen[¶], Paul P. Van Veldhoven[‖], Yasumaru Hatanaka[§2], and Tsuneo Imanaka[‡3]

From the [‡]Department of Biological Chemistry and [§]Laboratory of Biorecognition Chemistry, Graduate School of Medicine and Pharmaceutical Sciences, University of Toyama, 2630 Sugitani, Toyama 930-0194, Japan, the [¶]Department of Biochemistry and Biocenter Oulu, University of Oulu, P. O. Box 3000, FIN-90014, Finland, and the [‖]Department of Molecular Cell Biology, LIPIT, Katholieke Universiteit Leuven, Herestraat 49, B-3000 Leuven, Belgium

Peroxisomes play an essential role in a number of important metabolic pathways including β-oxidation of fatty acids and their derivatives. Therefore, peroxisomes possess various β-oxidation enzymes and specialized fatty acid transport systems. However, the molecular mechanisms of these proteins, especially in terms of substrate binding, are still unknown. In this study, to identify the substrate-binding sites of these proteins, we synthesized a photoreactive palmitic acid analogue bearing a diazirine moiety as a photophore, and performed photoaffinity labeling of purified rat liver peroxisomes. As a result, an 80-kDa peroxisomal protein was specifically labeled by the photoaffinity ligand, and the labeling efficiency competitively decreased in the presence of palmitoyl-CoA. Mass spectrometric analysis identified the 80-kDa protein as peroxisomal multifunctional enzyme type 2 (MFE2), one of the peroxisomal β-oxidation enzymes. Recombinant rat MFE2 was also labeled by the photoaffinity ligand, and mass spectrometric analysis revealed that a fragment of rat MFE2 (residues Trp^{249} to Arg^{251}) was labeled by the ligand. MFE2 mutants bearing these residues, MFE2(W249A) and MFE2(R251A), exhibited decreased labeling efficiency. Furthermore, MFE2(W249G), which corresponds to one of the disease-causing mutations in human MFE2, also exhibited a decreased efficiency. Based on the crystal structure of rat MFE2, these residues are located on the top of a hydrophobic cavity leading to an active site of MFE2. These data suggest that MFE2 anchors its substrate around the region from Trp^{249} to Arg^{251} and positions the substrate along the hydrophobic cavity in the proper direction toward the catalytic center.

Peroxisomes are organelles bound by a single membrane, which are present in almost all eukaryotic cells. Peroxisomes are involved in a variety of important metabolic processes including the β-oxidation of fatty acids, synthesis of plasmalogen, and bile acids (1). A specialized set of enzymes responsible for the peroxisomal functions are compartmentalized in the organelle, and the deficiency of peroxisomal enzymes causes severe metabolic disease such as acyl-CoA oxidase deficiency and D-bifunctional protein deficiency (2–4). Fibroblasts from patients with these deficiencies exhibit the disturbed peroxisomal β-oxidation of very long-chain fatty acids (VLCFAs),[4] and VLCFAs are accumulated in the plasma and tissues of these patients (5). Analyses of these peroxisomal diseases reflect the importance of the peroxisomal β-oxidation in organisms along with disclosing the enzymatic organization of the peroxisomal β-oxidation system. Peroxisomes are involved in the β-oxidation of VLCFAs, branched chain fatty acids such as pristanic acid, and bile acid intermediates such as dihydroxycholestanoic acid and trihydroxycholestanoic acid, which are incompatible with mitochondrial β-oxidation (6). Peroxisomal β-oxidation of fatty acids proceeds via a four-step pathway as in mitochondria, and multiple enzymes are involved in each step of the pathway. The first step of peroxisomal β-oxidation is the desaturation of acyl-CoA to the corresponding 2*E*-enoyl-CoA. In mammals, acyl-CoA oxidase 1 (ACOX1) oxidizes straight chain acyl-CoAs, whereas trihydroxycholestanoyl-CoA oxidase (ACOX2) and pristanoyl-CoA oxidase (ACOX3) oxidize both straight and 2-methyl-branched acyl-CoAs (7, 8). The second and third reactions are catalyzed by two multifunctional enzymes (MFEs) by stereochemically distinct pathways. MFE1 hydrates 2*E*-enoyl-CoA to 3*S*-hydroxyacyl-CoA and subsequently dehydrogenates the 3*S*-hydroxyacyl-CoA to 3-ketoacyl-CoAs, which is a naturally occurring pathway in the β-oxidation of straight chain fatty acids (9, 10). MFE2, the other peroxisomal multifunctional enzyme, which also possesses 2*E*-enoyl-CoA hydratase and 3-hydroxyacyl-CoA dehydrogenase activities, converts the 2*E*-enoyl-CoA into the corresponding 3-ketoacyl-CoA via a 3*R*-hydroxyacyl-CoA intermediate

* This work was supported in part by Grants-in-aid for the Research on Measures for Intractable Diseases from the Ministry of Health, Labour and Welfare of Japan and for Scientific Research from the Ministry of Education, Culture, Sports, Science and Technology of Japan (18590049, 18790050, 18390036, and 20390032). This work also supported in part by grants from CLUSTER (Cooperative Link of Unique Science and Technology for Economy Revitalization) and the Fugaku Trust for Medicinal Research.

[S] The on-line version of this article (available at http://www.jbc.org) contains supplemental Figs. S1 and S2 and Table S1.

[1] Both authors contributed equally to this work.

[2] To whom correspondence may be addressed. Tel.: 81-76-434-7515; Fax: 81-76-434-5063; E-mail: yasu@pha.u-toyama.ac.jp.

[3] To whom correspondence may be addressed. Tel.: 81-76-434-7545; Fax: 81-76-434-7545; E-mail: imanaka@pha.u-toyama.ac.jp.

[4] The abbreviations used are: VLCFA, very long-chain fatty acid; ACOX, acyl-CoA oxidase; H2, 2*E*-enoyl-CoA hydratase; HD, 3*R*-hydroxyacyl-CoA dehydrogenase; LCFA, long-chain fatty acid; MFE1 and MFE2, multifunctional enzyme type 1 and type 2; PMP70, 70-kDa peroxisomal membrane protein.

(11–15). MFE2 has a broad substrate spectrum, and is able to hydrate the enoyl-CoA esters of straight chain fatty acids, 2-methyl-branched fatty acids, and bile acid intermediates, and it can dehydrogenate the straight chain and branched chain 3-hydroxyacyl-CoAs (14, 16–19). The final step in peroxisomal β-oxidation is the thiolytic cleavage of 3-ketoacyl-CoAs into chain-shortened acyl-CoAs and acetyl-CoA or propionyl-CoA. It can be catalyzed by 3-ketoacyl-CoA thiolase or sterol carrier protein x, which cleaves straight chain ketoacyl-CoAs or both straight and 2-methyl-3-ketoacyl-CoAs, respectively (20). In addition to these enzymes, peroxisomes contain other important proteins that are directly or indirectly involved in the β-oxidation.

In terms of the transport of fatty acid derivatives destined for peroxisomal β-oxidation and their metabolites across the peroxisomal membrane, peroxisomal ATP-binding cassette proteins are suggested to be involved in this process. To date, three ATP-binding cassette transporters have been identified on mammalian peroxisomal membranes: the 70-kDa peroxisomal membrane protein (PMP70) (21–23), adrenoleukodystrophy protein (24), and adrenoleukodystrophy protein related protein (25, 26). A defect in adrenoleukodystrophy protein is known to be responsible for the X-linked neurodegeneration disorder, adrenoleukodystrophy. Adrenoleukodystrophy patient fibroblasts exhibit decreased β-oxidation of VLCFA, and VLCFA is accumulated in plasma and tissues (27, 28). Furthermore, we have reported that PMP70 is involved in the metabolic transport of long-chain acyl-CoA across peroxisomal membranes, based on studies with CHO cells overexpressing wild- and mutant-type PMP70 (29).

The enzymatic organization of the peroxisomal β-oxidation system and peroxisomal fatty acid transport system has been made relatively clear. However, the precise molecular mechanisms of these proteins, especially in terms of substrate recognition, are poorly understood. In this study, we synthesized a photoreactive palmitic acid analogue bearing a diazirine moiety as a photophore, and performed a photochemical approach with the novel photoreactive fatty acid analogue to identify fatty acid-binding proteins and analyze the substrate binding of the peroxisomal proteins.

EXPERIMENTAL PROCEDURES

Materials

pET21a was obtained from Novagen (Madison, WI). Talon metal affinity resin was purchased from Clontech (Palo Alto, CA). Nycodenz was from Axis-Shield (Oslo, Norway). Streptavidin-conjugated horseradish peroxidase was purchased from GE Healthcare. SoftLink SoftRelease Avidin Resin and sequencing grade modified trypsin were obtained from Promega (Madison, WI). α-Cyano-4-hydroxycinnamic acid was from Sigma. Mouse anti-His G antibody was purchased from Invitrogen. Preparation of the antibody against the COOH-terminal 15 amino acids of rat PMP70 is described in Ref.30.

Synthesis of Photoreactive Palmitoyl Acid Analogue Bearing Diazirine Moiety as a Photophore (Fig. 1)

N-(Diphenylmethylene)-3-[2-[2-[2-(2-tert-butoxylcarbonylaminoethoxy)ethoxy]ethoxy]-4-[3-(trifluoromethyl)-3H-diazirin-3-yl]phenyl]-L-alanine tert-Butyl Ester (2)—*tert*-Butylglycinate benzophenone imine (0.36 g, 1.2 mmol) and *O*-allyl-*N*-9-anthracenylmethylcinchonidium bromide (31) (0.06 g, 0.1 mmol) were dissolved in CH_2Cl_2 (7 ml) and the mixture was then cooled at −78 °C under nitrogen. 2-*tert*-Butylimino-2-diethylamino-1,3-dimethylperhydro-1,3,2-diazaphosphorine (0.5 g, 1.8 mmol) in CH_2Cl_2 (1 ml) and 2-[2-[2-(2-*tert*-butoxylcarbonylaminoethoxy)ethoxy]ethoxy]-4-[3-(trifluoromethyl)-*3H*-diazirin-3-yl]benzyl bromide (32) (0.55 g, 1 mmol) in CH_2Cl_2 (2 ml) were slowly added to the mixture followed by stirring for an additional 7 h. After removal of the solvent, the residue was dissolved in ether. The solution was washed with water twice and brine and dried over $MgSO_4$. The crude product was purified by column chromatography on silica gel (hexane:EtOAc = 1:1) to afford compound **2** (0.63 g, 85%) as a pale yellow oil; ^{1}H NMR ($CDCl_3$) δ 7.50–7.52 (m, 2H), 7.22–7.38 (m, 6H), 7.10 (d, 1H, *J* = 7.7 Hz), 6.62 (d, 1H, *J* = 7.7 Hz), 6.54 (br s, 2H), 6.48 (s, 1H), 5.02 (br s, 1H), 4.26 (dd, 1H, *J* = 3.4, 9.8 Hz), 3.92 (m, 1H), 3.50–3.62 (m, 9H), 3.36 (dd, 1H, *J* = 3.4, 13.2 Hz), 3.32 (br q, 2H, *J* = 5.1 Hz), 3.01 (dd, 1H, *J* = 9.8, 13.2 Hz), 1.45 (s, 9H), 1.44 (s, 9H).

3-[2-[2-[2-(2-tert-Butoxylcarbonylaminoethoxy)ethoxy]-ethoxy]-4-[3-(trifluoromethyl)-3H-diazirin-3-yl]phenyl]-L-alanine tert-Butyl Ester (3)—An 80% ethanol solution of NH_2OH/HCl (1 M, 5 ml) was added to a solution of compound **2** (0.66 g, 0.81 mmol) in CH_2Cl_2 (5 ml). The reaction mixture was stirred at 45 °C for 1 h. After removal of the solvent, the residue was dissolved in CH_2Cl_2 and purified by column chromatography on silica gel (CH_2Cl_2:methanol = 10:1) to afford compound **3** (0.44 g, 92%) as a pale yellow oil; ^{1}H NMR ($CDCl_3$) δ 7.16 (d, 1H, *J* = 7.7 Hz), 6.75 (d, 1H, *J* = 7.7 Hz), 6.60 (s, 1H), 5.36 (br s, 1H), 4.18 (ddd, 1H, *J* = 3.4, 7.3, 9.8 Hz), 4.12 (ddd, 1H, *J* = 3.4, 5.1, 9.8 Hz), 4.02 (br s, 1H), 3.89 (br s, 1H), 3.83 (ddd, 1H, *J* = 3.4, 5.1, 11.1 Hz), 3.77–3.80 (m, 1H), 3.69 (m, 1H), 3.63–3.66 (m, 2H), 3.55–3.60 (m, 1H), 3.49–3.54 (m, 1H), 3.33 (br s, 2H), 3.27 (br s, 1H), 2.91 (dd, 1H, *J* = 8.3, 13.9 Hz), 1.42 (s, 9H), 1.34 (s, 9H).

N-Palmitoyl-3-[2-[2-[2-(2-tert-butoxylcarbonylaminoethoxy)ethoxy]ethoxy]-4-[3-(trifluoromethyl)-3H-diazirin-3-yl]phenyl]-L-alanine tert-Butyl Ester (4)—A CH_2Cl_2 solution (1 ml) of compound **3** (200 mg, 0.35 mmol) was added to a CH_2Cl_2 solution (3 ml) of palmitic acid (90 mg, 0.35 mmol), 1-(3-dimethylaminopropyl)-3-ethylcarbodiimide (74 mg, 0.38 mmol), and Et_3N (39 mg, 0.38 mmol). The reaction mixture was stirred overnight at room temperature. After removal of the solvent, the residue was purified by column chromatography on silica gel (hexane:EtOAc = 1:1) to afford compound **4** (223 mg, 79%) as a pale yellow solid; ^{1}H NMR ($CDCl_3$) δ 7.17 (d, 1H, *J* = 7.7 Hz), 6.73 (d, 1H, *J* = 7.7 Hz), 6.59 (s, 1H), 6.37 (d, 2H, *J* = 8.1 Hz), 5.12 (br s, 1H), 4.71–4.77 (m, 1H), 4.08–4.18 (m, 2H), 3.88–3.96 (m, 2H), 3.71–3.79 (m, 2H), 3.67 (t, 2H, *J* = 4.7 Hz), 3.55 (t, 2H, *J* = 5.1 Hz), 3.31 (q, 2H, *J* = 5.1 Hz), 3.07 (dd, 1H, *J* = 9.6, 13.5 Hz), 2.98 (dd, 1H, *J* = 5.8, 13.5 Hz), 2.04–2.14 (m, 2H), 1.40–1.50 (m, 11H), 1.38 (s, 9H), 1.12–1.32 (m, 26H), 0.88 (t, 3H, *J* = 6.8 Hz).

N-Palmitoyl-3-[2-[2-[2-(2-aminoethoxy)ethoxy]ethoxy]-4-[3-(trifluoromethyl)-3H-diazirin-3-yl]]-phenylalanine (5)—Deprotection of compound **4** (0.20 g, 0.25 mmol) was performed with 50% TFA-$CHCl_3$ (4 ml) at room temperature.

After stirring for 3 h, the solvent was removed. The product was extracted with $CHCl_3$ three times from aqueous $NaHCO_3$ solution. The organic solution was combined, washed twice with brine, and then dried over $MgSO_4$ to afford compound **5** (0.16 g quantity) as a pale yellow solid. Removal of the two *tert*-butyl groups was confirmed by NMR and the product was used without further purification; ^{1}H NMR ($CDCl_3$) δ 7.21 (d, 1H, J = 7.8 Hz), 6.81 (br s, 1H), 6.69 (d, 1H, J = 7.8 Hz), 6.51 (s, 1H), 4.52 (br s, 1H), 4.07–4.16 (m, 2H), 3.89–3.95 (m, 1H), 3.75–3.86 (m, 2H), 3.64–3.75 (m, 5H), 2.91–3.17 (m, 4H), 2.00–2.09 (m, 4H), 1.11–1.38 (m, 26H), 1.00–1.10 (m, 2H), 0.88 (t, 3H, J = 7.1 Hz).

N-Palmitoyl-3-[2-[2-[2-(2-biotinylaminoethoxy)ethoxy]-ethoxy]-4-[3-(trifluoromethyl)-3H-diazirin-3-yl]]-phenylalanine (1)—A solution of NHS-biotin (88 mg, 0.26 mmol) in *N,N*-dimethylformamide (3 ml) was added to a solution of compound **5** (160 mg, 0.24 mmol) and Et_3N (26 mg, 0.26 mmol) in $CHCl_3$ (3 ml), and the reaction mixture was stirred overnight at room temperature under nitrogen. After removal of the solvent the residue was purified by column chromatography on silica gel ($CHCl_3$:methanol = 5:1) to afford compound **1** (158 mg, 74%) as a pale yellow solid; ^{1}H NMR (5% CD_3OD-$CDCl_3$) δ 7.21 (d, 1H, J = 7.7 Hz), 6.74 (d, 1H, J = 7.7 Hz), 4.63 (dd, 1H, J = 5.1, 9.4 Hz), 4.49–4.53 (m, 1H), 4.51 (dd, 1H, J = 4.3, 7.7 Hz), 4.12–4.15 (m, 2H), 3.87–3.96 (m, 2H), 3.73–3.76 (m, 2H), 3.65–3.69 (m, 2H), 3.56–3.62 (m, 2H), 3.41–3.47 (m, 1H), 3.33–3.39 (m, 1H), 3.19 (dd, 1H, J = 5.1, 13.7 Hz), 3.15 (dd, 1H, J = 4.3, 7.3 Hz), 3.02 (dd, 1H, J = 9.4, 13.7 Hz), 2.92 (dd, 1H, J = 5.1, 12.8 Hz), 2.73 (dd, 1H, J = 6.4, 12.8 Hz), 2.18 (t, 2H, J = 6.8 Hz), 2.09 (t, 2H, J = 7.7 Hz), 1.55–1.70 (m, 4H), 1.37–1.45 (m, 4H), 1.18–1.32 (m, 24H), 1.09–1.16 (m, 2H), 0.88 (t, 3H, J = 6.8 Hz).

Preparation of Rat Liver Peroxisomes

The livers of male Wister rats were fractionated by the methods of de Duve *et al.* (33). The livers were homogenized in 4 volumes of SVEH (0.25 M sucrose, 1 mM EDTA, 0.1% ethanol, and 5 mM Hepes-KOH, pH 7.4), and the supernatant (post-nuclear supernatant) was recovered by centrifugation at 1,000 × *g* for 10 min at 4 °C. The heavy and light mitochondrial fraction was sedimented from the post-nuclear supernatant fraction by centrifugation at 20,000 × *g* for 22 min. About 0.7 ml of the light mitochondrial fraction was applied onto a 10-ml linear Nycodenz gradient (density span from 1.15–1.25 g/ml in SVEH), and centrifuged 193,000 × *g* for 2 h at 4 °C. Fractions of ~1.0 ml were collected in preweighed microtubes, and the density of each fraction was determined by refractometry. The peroxisomal fraction was identified by the density and distribution of catalase (33).

Plasmid Construction

The full-length MFE2 cDNA was obtained from the plasmid pUC18/rat MFE2 (34) by PCR amplification using the primer pair: 5′-GCTAGCCCTCTGAGGTTCGACGGG-3′ (the NheI site is underlined) and 5′-CTCGAGCTTGGCATAGTCTTTCAG-3′ (the XhoI site is underlined). The PCR-generated fragment containing NheI and XhoI restriction sites was inserted at the corresponding sites of pET21a, a C-terminal histidine tag fusion protein expression vector, to construct pET21a/MFE2. The identity of the construction was confirmed by semiautomated sequencing on an ABI 310 DNA sequencer (PerkinElmer Life Science).

Site-directed Mutagenesis of MFE2

Site-directed mutagenesis was performed on pET21a/MFE2 using a QuikChange site-directed mutagenesis kit (Stratagene) according to the manufacturer's instructions. The oligonucleotide primers used were designed on the basis of their sequences (supplemental Table S1). The mutations in the constructions were confirmed by sequencing.

Purification of MFE2-His

Overexpression and purification of recombinant MFE2 was performed as described by Haapalainen *et al.* (34) with some modifications. Details are shown under the supplemental data.

Photoaffinity Labeling

The photoprobe (10 nmol) was dissolved in $CHCl_3$, and the solvent was evaporated by nitrogen gas stream to deposit the probe on the wall of glass test tube as a thin film. Binding buffer (25 mM Tris-HCl, pH 7.8, 300 mM NaCl, 5 mM EDTA, and 1 mM DTT) containing 2 mg/ml of BSA was then added to make up a 20 μM probe solution and then mixed by vortex. In a typical experiment, rat liver peroxisomes (100 μg of protein) or purified MFE2-His (10 μg of protein) were suspended in a final volume of 0.1 ml of binding buffer. The photoprobe solution was then added to the suspension to a final concentration of 2 μM, and the reaction mixtures were incubated at 4 °C for 2 h. After UV irradiation with 30 W/m^2 of 360 nm light for 20 min at 0 °C, samples were subjected to SDS-PAGE and transferred onto a PVDF membrane. The labeled proteins were detected by a chemiluminescent method using streptavidin-conjugated horseradish peroxidase.

MALDI-TOF Analysis of the Labeled Protein

After photoaffinity labeling of purified MFE2-His (100 μg of protein), the reaction product was applied onto SoftLink Soft Release Avidin Resin equilibrated with the binding buffer. After incubation of the suspensions for 2 h at 4 °C, the beads were collected by centrifugation and washed five times with 250 μl of the binding buffer. Labeled proteins were eluted by 2 × sample buffer for SDS-PAGE (4% (w/v) SDS, 19.8% (v/v) sucrose, 0.08 M Tris-HCl, pH 6.8, 20 mM DTT, and 0.002% (w/v) bromphenol blue), and separated on a 5–10% SDS-polyacrylamide gradient gel. After electrophoresis, labeled proteins were transferred onto a PVDF membrane, stained with Coomassie Brilliant Blue, destained, and then the bands corresponding to the labeled proteins were excised from the membrane. The membrane fragments were incubated for 1 h at 27 °C with reduction buffer (0.5 M Tris, pH 8.5, 8 M guanidinium HCl, 0.3%(w/v) EDTA, and 5% acetonitrile) containing 10 mg/ml of DTT and then for 20 min in the same buffer containing 30 mg/ml of iodoacetamide. The *S*-carboxyamidomethylated sample was soaked in 100 μl of digestion buffer (50 mM NH_4HCO_3, pH 8.0, and 70% acetonitrile), and digested with 2 μg of sequencing-grade modified trypsin for 12 h at 27 °C. The digestion was terminated by the addition of PMSF to 10 μM of the final concentration and the sample was concentrated in a SpeedVac concentrator (Savant,

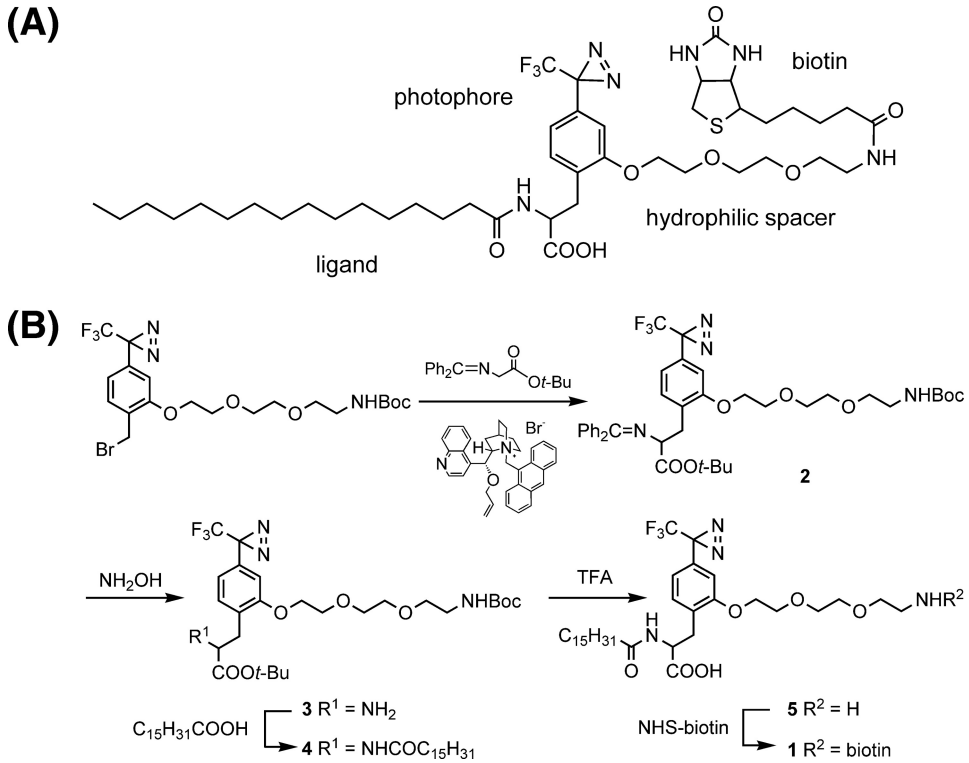

FIGURE 1. **Synthesis of photoreactive LCFA probe.** *A*, structure of the photoreactive LCFA probe. *B*, synthetic scheme for the preparation of the photoreactive LCFA probe.

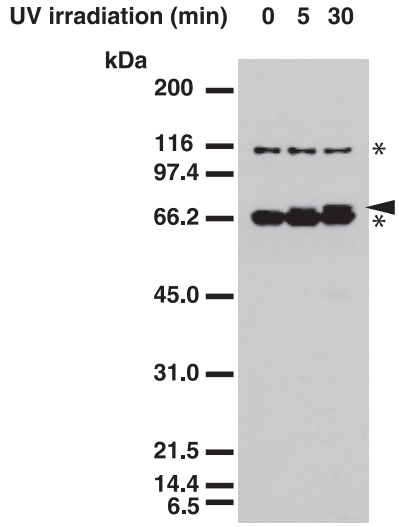

FIGURE 2. **Photoaffinity labeling of rat liver peroxisomes.** Purified rat liver peroxisomes (100 μg of protein) were incubated with the photoreactive LCFA probe for 2 h at 4 °C. After UV irradiation at 360 nm for 0–30 min at 0 °C, labeled proteins were separated on a 7–15% SDS-polyacrylamide gradient gel, and detected by streptavidin-HRP. The *arrowhead* indicates the 80-kDa protein labeled by the photoaffinity probe. *Asterisks* indicate nonspecific bands.

Farmingdale, NY). The resulting residue was resuspended in 10 μl of 0.1% TFA. The tryptic peptide mixture was desalted with Zip Tip (Millipore, Billerica, MA) and eluted in 2 μl of 33.3% acetonitrile with 0.06% TFA. The recovered tryptic peptides (1 μl) were mixed with 1 μl of a 10 mg/ml solution of α-cyano-4-hydroxycinnamic acid in 33.3% acetonitrile with 0.06% TFA and analyzed by MALDI-TOF mass spectrometry on a Bruker MALDI-TOF AutoFlex mass spectrometer (Bruker-Daltonics, Billerica, MA).

Other Methods

Protein was assayed as described previously (29). Western blot analysis was performed using primary antibodies and a secondary antibody, donkey anti-rabbit or anti-mouse IgG antibody-conjugated horseradish peroxidase (GE Healthcare). Antigen-antibody complex was visualized with ECL+ Western blotting detection reagent (GE Healthcare).

RESULTS

Chemistry—To identify and characterize long-chain fatty acid (LCFA)-binding proteins in peroxisomes, we synthesized a novel photoreactive LCFA probe **1** (Fig. 1*A*). The synthetic probe consists of a LCFA, a diazirine-based photophore, and a biotin moiety with a hydrophilic linker. The (3-trifluoromethyl)phenyldiazirine is one of the most promising photophores. By photoirradiation, it produces a carbene species, a highly reactive intermediate, and immediately makes a covalent bond with spatially close molecules. A biotin moiety was directly anchored to the photophore via a hydrophilic linker as a tag for the detection and isolation of labeled proteins utilizing biotin-avidin interaction, and is also useful for identifying the labeled protein and its ligand-interacting site. For preparation of a photoreactive fatty acid analogue, a phenylalanine analogue has been employed to introduce a diazirine photophore with an accompanying carboxylate at the end of palmitic acid (16:0). Preparation of the photoreactive phenylalanine derivative was achieved in excellent yield according to the previous method (35). The coupling reaction with palmitic acid and the subsequent biotinylation to give the corresponding photoreactive fatty acid probe **1** is outlined in Fig. 1*B*.

Photoaffinity Labeling of Rat Liver Peroxisomes—Using the photoreactive LCFA analogue as a probe, we performed photoaffinity labeling experiments on purified rat liver peroxisomes. Purified rat liver peroxisomes were incubated with the photoreactive fatty acid analogue, and the labeled proteins were separated on a 7–15% SDS-polyacrylamide gradient gel, and then detected by streptavidin-HRP. As shown in Fig. 2, an 80-kDa protein was specifically labeled by the probe upon activation with UV irradiation. The efficiency of the labeling of the 80-kDa protein increased with the irradiation time. In addition to the 80-kDa protein, two bands with molecular masses of 110 and 70 kDa, respectively, were also detected by streptavidin-HRP. However, these two bands were detected even in the non-irradiated sample, suggesting that these two proteins were not photolabeled products, but nonspecifically reacted with streptavidin-HRP.

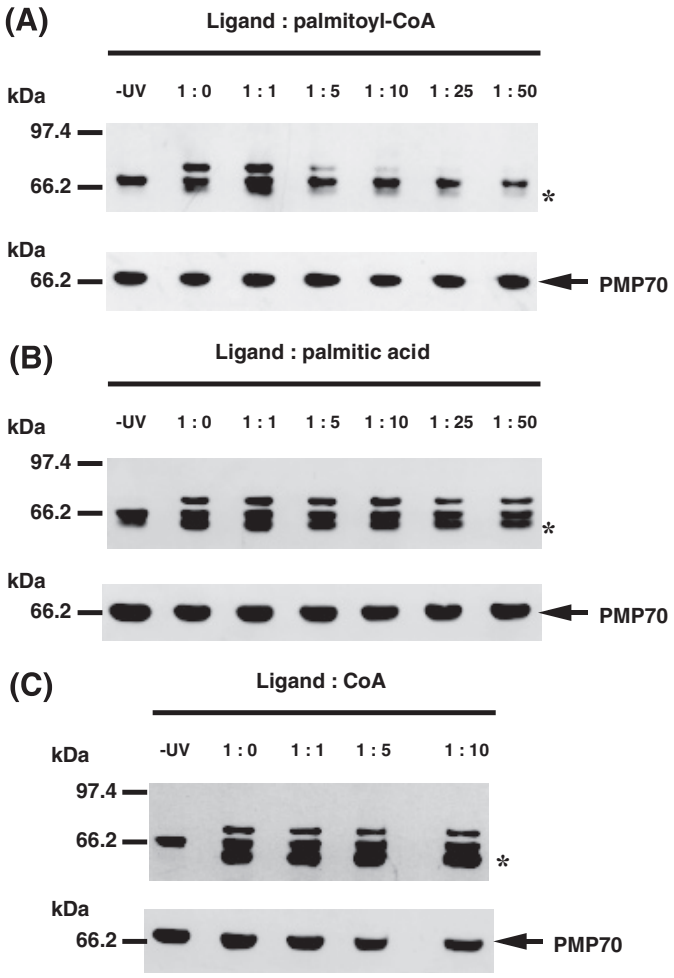

FIGURE 3. **Photoaffinity labeling of rat liver peroxisomes in the presence of palmitoyl-CoA, palmitic acid, and CoA.** Purified rat liver peroxisomes were photoaffinity labeled in the presence of increasing amounts of palmitoyl-CoA (*A*), palmitic acid (*B*), and CoA (*C*), respectively. After UV irradiation, labeled proteins were separated on a 7–15% SDS-polyacrylamide gradient gel, and detected by streptavidin-HRP (*upper panels*). Western blot analysis for PMP70 is used as a loading control (*lower panels*). The *arrowheads* and *asterisks* indicate the 80-kDa protein and the 65-kDa protein labeled by the photoaffinity probe, respectively.

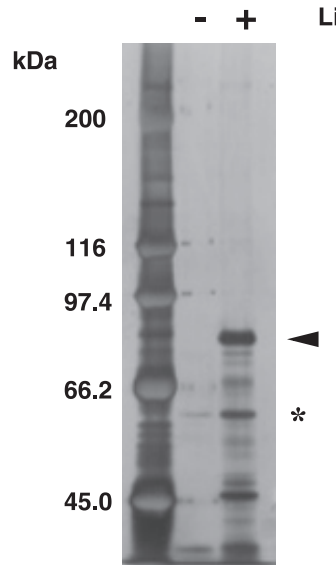

FIGURE 4. **Purification of the photolabeled 80-kDa protein.** Purified rat liver peroxisomes (1 mg of protein) were labeled by the photoreactive LCFA probe. After solubilization with 0.1% Triton X-100, labeled proteins were purified by SoftLink Soft Release Avidin Resin. Purified proteins were separated on a 5–10% SDS-polyacrylamide gradient gel, and stained with silver staining. The *arrowhead* and *asterisk* indicates the 80- and 65-kDa proteins labeled by the photoaffinity probe, respectively.

Next, to characterize the binding specificity of the probe to the 80-kDa protein, we examined the competitive effects of palmitoyl-CoA, palmitic acid, and CoA on the photoaffinity labeling of the 80-kDa protein. As shown in Fig. 3*A*, the probe photoincorporation within the 80-kDa protein was suppressed by the presence of palmitoyl-CoA in a concentration-dependent manner. On the other hand, the labeling was not inhibited even in the presence of an excess amount of palmitic acid or CoA (Fig. 3, *B* and *C*). These data indicate that the 80-kDa protein has a potent capacity to interact with palmitoyl-CoA, and the photoreactive LCFA probe could bind to the 80-kDa protein in the region responsible for its palmitoyl-CoA-binding site.

Identification of the 80-kDa Protein—In preliminary experiments, the 80-kDa protein labeled by the photoaffinity probe was susceptible to extraction with sodium carbonate, and was protected from digestion with trypsin in the absence of Triton X-100, but degraded by trypsin in the presence of Triton X-100 (data not shown). These behaviors were not similar to those of PMP70, a peroxisomal membrane protein, but resembled those of catalase, a peroxisomal matrix protein, implying that the 80-kDa protein is located in the peroxisomal matrix. To identify the 80-kDa protein, peroxisomes were solubilized with 0.1% Triton X-100 after photoaffinity labeling, and the labeled proteins were isolated by streptavidin-agarose resin. As shown in Fig. 4, the 80-kDa protein was successively purified. The purified probe-incorporated 80-kDa protein was digested with trypsin, and the resulting tryptic peptide mixture was analyzed by MALDI-TOF mass spectrometry. As a result, several specific tryptic peptide fragments of the labeled protein were obtained, and the MASCOT search engine revealed that almost all of the major fragments correspond to MFE2-specific tryptic fragments (supplemental Fig. S1). In addition to these fragments, a characteristic peak was observed at m/z 1345.81. We assigned the fragment as a photoadduct fragment (details are shown below).

Together with MFE2, a 65-kDa protein was also purified by streptavidin-agarose resin (Fig. 4). The 65-kDa protein was indeed labeled by the LCFA probe and the labeling of the 65-kDa protein was competitively inhibited by the presence of palmitoyl-CoA with almost the same extent as that of MFE2 (Fig. 3). Accompanying with intact MFE2, the 65-kDa protein was also detected in the purified rat liver peroxisomes by immunoblotting using anti-MFE2 antibody (data not shown). These data indicate that MFE2 is partially degraded to the 65-kDa protein and the 65-kDa region of MFE2 still possesses a potent capacity to interact with palmitoyl-CoA and the photoreactive LCFA probe.

MFE2, also called multifunctional protein 2 or D-bifunctional protein, is a 79-kDa enzyme that possesses a typical peroxisomal matrix protein targeting signal (COOH-terminal Ala-Lys-Leu). MFE2 consists of a 3*R*-hydroxyacyl-CoA dehydrogenase

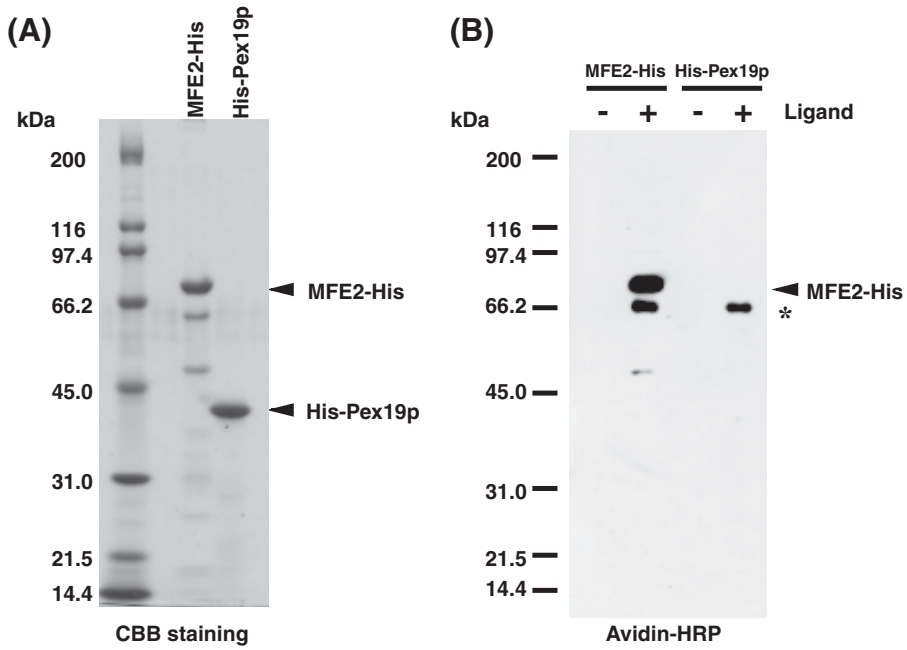

FIGURE 5. **Photoaffinity labeling of purified MFE2-His.** Purified MFE2-His and His-Pex19p (*A*) were incubated with the photoreactive LCFA probe for 2 h at 4 °C. After UV irradiation at 360 nm for 30 min at 0 °C, labeled proteins were separated on a 7–15% SDS-polyacrylamide gradient gel, and detected by streptavidin-HRP (*B*). The *asterisk* indicates nonspecific bands.

(HD) domain, a 2*E*-enoyl-CoA hydratase 2 (H2) domain, and a sterol carrier protein 2-like domain, and is known to catalyze the second and third steps of the peroxisomal β-oxidation of fatty acids and their derivatives (36).

Purification and Photoaffinity Labeling of MFE2—COOH-terminal His_6-tagged rat MFE2 (MFE2-His) was expressed in *Escherichia coli* and purified with Talon metal affinity resin. MFE2-His was expressed upon isopropyl-β-D-thiogalactopyranoside induction as a major protein and exclusively recovered in a soluble form. MFE2-His purified from the soluble fraction was >80% pure as judged by SDS-PAGE (supplemental Fig. S2*A*). It is suggested that rat MFE2 functions as a homodimer. Therefore, we analyzed the oligomeric state of purified MFE2 using sucrose density gradient centrifugation. The molecular mass of the purified MFE2-His was estimated to be 155 kDa on sucrose density gradient centrifugation, which almost corresponded to a dimeric form of MFE2-His (79.4 kDa) (supplemental Fig. S2*B*). The purified MFE2-His was subjected to photoaffinity labeling with the photoreactive LCFA probe. As shown in Fig. 5, MFE2-His was efficiently labeled by the probe. On the other hand, purified His_6-tagged Pex19p (His-Pex19p), a cytosolic protein involved in the targeting of peroxisomal membrane proteins (37), was not labeled by the probe under the same conditions. These findings indicate that the photoaffinity ligand indeed incorporates into MFE2 with high specificity.

Identification of the Substrate-binding Site of MFE2—As mentioned above, the photoreactive LCFA probe bound to MFE2 at its palmitoyl-CoA-binding site. Therefore, we tried to identify the individual amino acid residues labeled by the probe within MFE2 to characterize the substrate-binding site of MFE2. MFE2-His was incubated with the probe and the labeled MFE2-His was purified by avidin resin. After digestion with trypsin, the resulting peptide mixture was analyzed by MALDI-TOF mass spectrometry. As shown in Fig. 6, various tryptic fragments with observed molecular masses that were compatible with the calculated molecular mass of MFE2 tryptic fragments were identified in samples prepared from both labeled and unlabeled MFE2. However, a peak at *m*/*z* 1345.39 was detected only in the sample prepared from labeled MFE2. The fragment was also detected in the cross-linked MFE2 purified from rat liver peroxisomes as described above (supplemental Fig. S1*A*). The molecular mass of the fragment did not agree with any of the theoretical MFE2 fragments digested with trypsin, instead, it matched exactly with the mass of the tryptic peptide of MFE2 (residues Trp^{249}-Glu^{250}-Arg^{251}; *m*/*z* 489.23) modified with the probe (*m*/*z* 1345.69 = 489.23 + 856.46). On the other hand, the tryptic fragment corresponding to MFE2 sequence Trp^{249}-Glu^{250}-Arg^{251} (*m*/*z* 489.24) was absent from the labeled MFE2-His, but observed in the control experiment using tryptic digestion of the unlabeled MFE2-His. To confirm that the amino acid region (Trp^{249}-Glu^{250}-Arg^{251}) within MFE2 is involved in ligand binding, we purified the MFE2 mutants by replacing these amino acids with Ala, and analyzed the ligand binding efficiency. As shown in Fig. 7, wild type MFE2 was labeled by the photoaffinity probe. However, MFE2(W249A) and MFE2(R251A) exhibited a decreased labeling efficiency. The 1abeling efficiencies of MFE2(W249A) and MFE2(R251A) with the probe decreased to ~30% compared with that of the wild type MFE2 (Fig. 7*C*). These three amino acid residues lie within the HD domain of MFE2, and a disease-causing mutation has been identified in this region (38). The mutant, MFE2(W249G), also exhibited a decreased labeling efficiency, whereas MFE2(N158D), another disease-causing mutant in which the mutated residue is situated outside of the labeled region (38), exhibited only a slightly affected labeling efficiency for the photoreactive LCFA probe under the same conditions. The purified MFE2 HD domain was also labeled by the photoaffinity ligand, and MFE2 HD(W249A) exhibited a decreased labeling efficiency. However, the ligand was incorporated in the purified HD domain very weakly compared with full-length MFE2 (data not shown). The ternary composition of the three domains of MFE2 is required for the efficient substrate binding of MFE2. These data indicate that the amino acid region within MFE2 (Trp^{249}-Glu^{250}-Arg^{251}) is important for ligand binding.

Characterization of the Substrate Binding Mode of MFE2—As described above, the photophore of the photoreactive LCFA probe cross-linked with MFE2 at the three amino acid regions of the MFE2 HD domain (Trp^{249}-Glu^{250}-Arg^{251}). The crystal

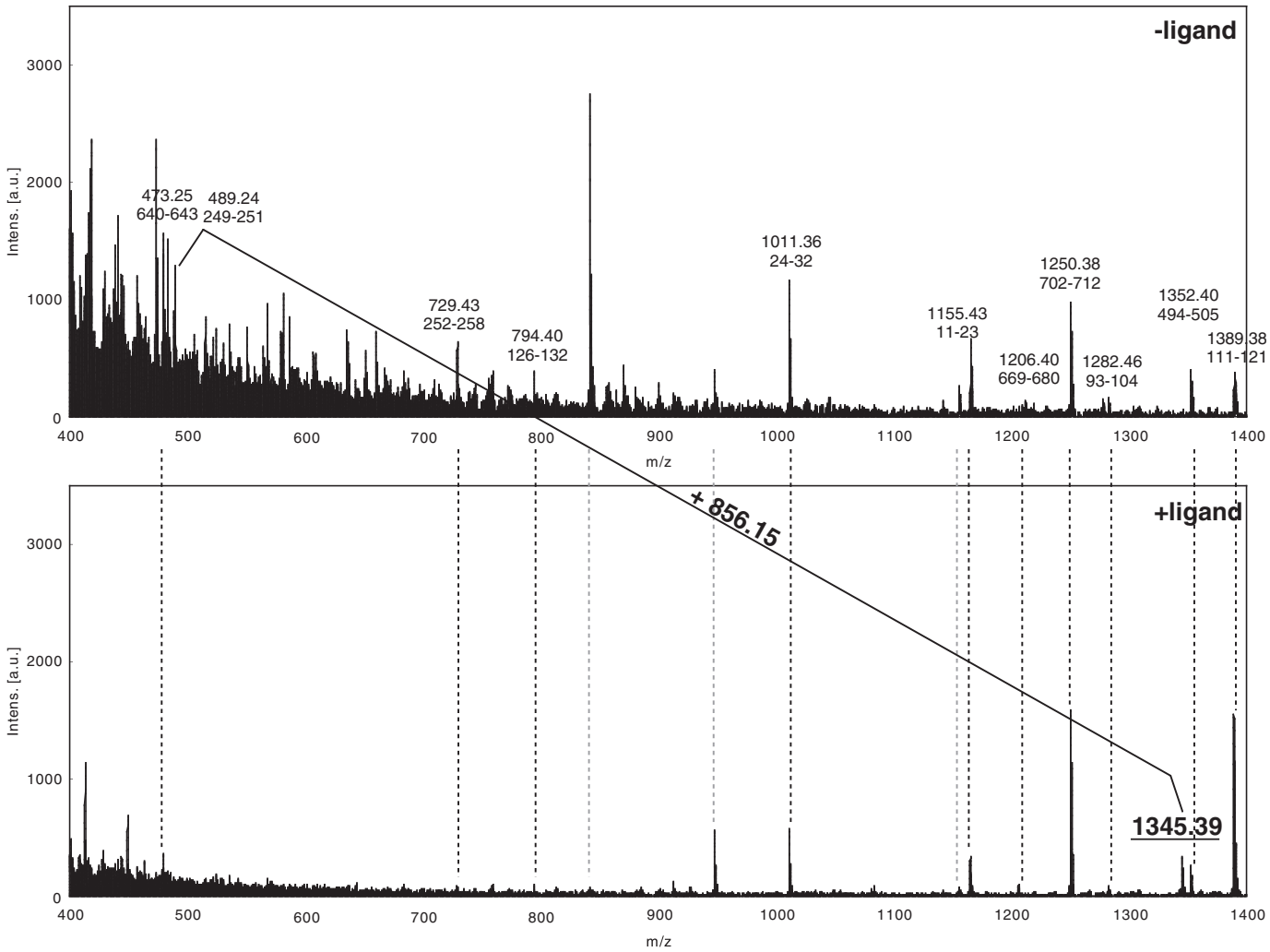

FIGURE 6. **Identification of the substrate-binding site of MFE2.** Purified MFE2-His (100 μg of protein) was incubated with the photoreactive LCFA probe. The probe-incorporated MFE2-His was isolated by avidin resin followed by trypsin digestion. The resulting tryptic peptide mixture was analyzed by MALDI-TOF mass spectrometry (*lower panel*). As a control, unlabeled MFE2-His was similarly digested with trypsin and the resulting tryptic peptide mixture was subjected onto MALDI-TOF mass spectrometry (*upper panel*). The *diagonal line* indicates the mass difference between the peak in control sample corresponding to unmodified MFE2-peptide (amino acids 249–251) and the peak corresponding to an adduct of the MFE2-peptide (amino acids 249–251) with the LCFA probe in the sample treated with the probe.

structure of the HD domain of rat MFE2 HD has been solved by Haapalainen *et al.* (34). Based on the three-dimensional structure, these residues lie on the β strand located on top of the dimerization interface of the subunits (Fig. 8*A*). The location is apart from the catalytic triad of MFE2 HD domain (Ser^{151}, Tyr^{164}, Lys^{168}). However, these residues also locate at the tip of the hydrophobic cavity leading to the active site (Fig. 8*B*). Therefore, we speculated that MFE2 could anchor the photophore of the LCFA derivative ligand on the top of the hydrophobic cavity (Trp^{249}-Glu^{250}-Arg^{251}) and bury the hydrophobic probe along with the hydrophobic cavity directing the fatty-acyl tail of the ligand toward the active site. To challenge this hypothetical substrate binding mode of MFE2 HD, we replaced the hydrophobic residues (Ile^{180}, Ile^{288}) and the aromatic residue (Tyr^{156}) forming the hydrophobic cavity of the MFE2 HD domain, and examined the photoaffinity labeling of these mutant proteins. As shown in Fig. 9, wild type MFE2 was labeled by the photoaffinity probe. However, MFE2(I180N), MFE2(I288N), and MFE2(Y156S) were impaired in the interaction with the photoreactive LCFA probe. These data indicate that the hydrophobic cavity leading to the active site of the MFE2 HD domain can be assigned as one of the substrate-binding sites of MFE2.

DISCUSSION

Peroxisomes play important roles in fatty acid metabolism. Therefore, they contain various enzymes involved in fatty acid metabolism and transport. However, because of the highly hydrophobic nature of the substrates, the precise mechanisms of their substrate recognition and binding has been poorly understood. In this study, we adopted a novel photochemical approach. We synthesized a photoreactive palmitic acid analogue bearing a diazirine moiety as a photophore, and characterized the molecular mechanisms especially in the substrate binding of peroxisomal β-oxidation enzymes by photoaffinity labeling using a novel photoreactive LCFA probe.

At first, we identified MFE2 as a ligand-binding protein based on the following observations. 1) The probe used in this study

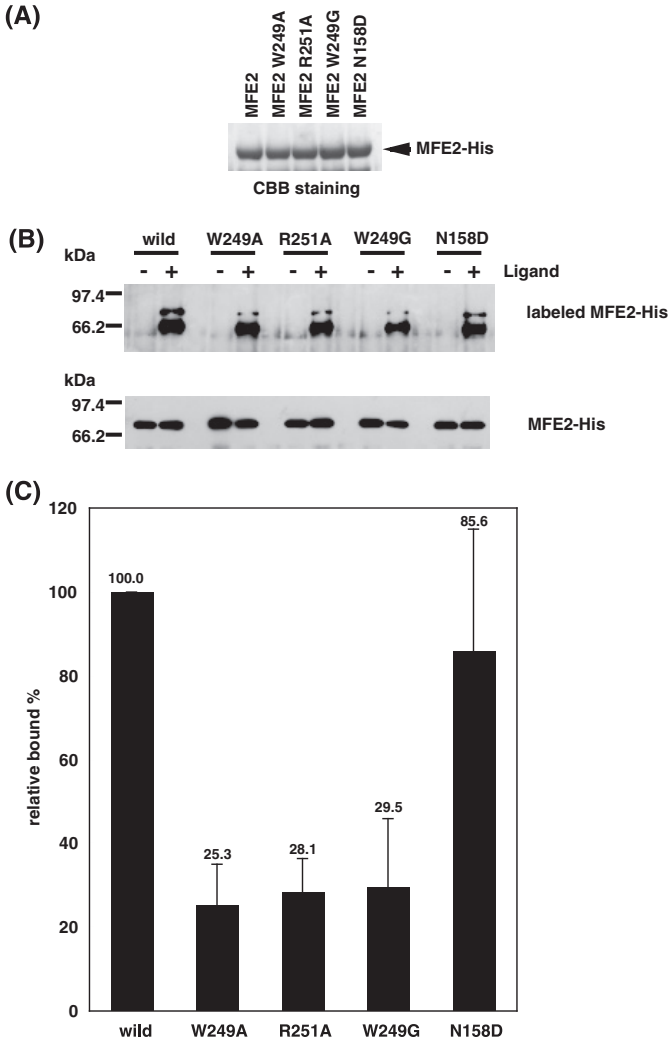

FIGURE 7. **Photoaffinity labeling of mutant MFE2-His.** *A*, comparison of the purities of mutant MFE2-His (10 μg of protein). *B*, wild type and mutant MFE2-His (3.9 μg of protein) were labeled by the photoreactive LCFA probe. The labeled proteins were separated on a 7–15% SDS-polyacrylamide gradient gel, and detected by streptavidin-HRP. *C*, the amount of probe-incorporated MFE2s shown in *B* was quantified with a LAS4000 luminoanalyzer (Fuji Film, Tokyo, Japan) and the relative labeling percentage was expressed as a ratio of the labeling percentage of each mutant MFE2 with that of wild type MFE2.

was specifically incorporated into an 80-kDa peroxisomal matrix protein upon activation with UV irradiation (Fig. 2), and the MALDI-TOF mass analysis identified the 80-kDa protein as peroxisomal MFE2 (supplemental Fig. S1). 2) Recombinant MFE2-His was specifically labeled by the photoreactive LCFA probe (Fig. 5). MFE2 catalyzes the second and third steps of peroxisomal β-oxidation of straight chain and branched chain fatty acids and bile acid intermediates. The patients with MFE2 deficiency and MFE2 knock-out mice showed accumulations of VLCFA, branched chain fatty acids, and bile acid intermediates (39–43). Jiang *et al.* (44) reported that MFE2 purified from rat liver exhibited hydratase/dehydrogenase activities on hexadecenoyl-CoA and 2-methylhexadecenoyl-CoA. In addition, although LCFA is largely degraded through the mitochondrial β-oxidation pathway, LCFA oxidation of MFE2-deficient human fibroblasts was lower than control fibroblasts under a condition in which the mitochondrial LCFA oxidation was inhibited (40). These data indicate that MFE2 could bind LCFA derivatives as substrates. Why was only MFE2 specifically labeled by the photoreactive LCFA probe among the peroxisomal proteins supposed to interact with fatty acid derivatives such as ACOX1? We do not know the exact reason at present. However, we presume a possible explanation as follows. The photoprobe used in this study is composed of LCFA moiety, a diazirine-based photophore, and a biotin moiety with a hydrophilic linker. The structure of the photoprobe is different from that of CoA, LCFA, and also LCFA-CoA. However, amphipathic characteristics of the photoprobe seem to resemble somehow that of LCFA-CoA. In addition, as mentioned above MFE2 shows broad substrate specificity to hydrophobic molecules. MFE2 can also accept medium chain fatty acyl-CoA, 17β-estradiol, and 5-androstene-3β,17β-diol (12, 16, 19, 44–46). Therefore, MFE2 could have a potent capacity to interact with the photoprobe at its substrate-binding site. On the other hand, acyl-CoA-binding proteins such as AOX1 did no bind the photoprobe because they probably recognize acyl-CoA more in a rigorous manner. To improve the limited utility of this ligand as LCFA-CoA probe, we are now trying to modify the structure and the position of the photophore and detection tag not to affect the nature of LCFA-CoA.

MFE2 is a matrix protein existing inside of peroxisomes. Therefore, the photoreactive LCFA probe must be imported into peroxisomes. We assessed the transport of the photoreactive LCFA probe across the peroxisomal membrane by limited trypsin digestion. The ligand-incorporated MFE2 was protected from trypsin digestion after photoaffinity labeling. However, photoaffinity labeling of MFE2 did not occur when ligand was incubated with peroxisomes pretreated with trypsin. Under this condition, peroxisomal membrane proteins were degraded but peroxisomal matrix proteins were not (data not shown). These data indicate that the ligand is transported into peroxisomes by peroxisomal membrane proteins. However, at present, we have not identified the peroxisomal membrane proteins that interact with this ligand.

Next, we characterized the substrate binding mode of MFE2. We suggest that MFE2 anchors its substrate around the region consisting of Trp^{249} to Arg^{251} and buries the substrate along the hydrophobic cavity in the proper direction toward the catalytic center of the MFE2 HD domain based on the following observations. 1) MFE2 was labeled by the photoreactive LCFA probe, and the labeling was competitively inhibited in the presence of palmitoyl-CoA (Fig. 3). 2) MALDI-TOF mass analysis identified three amino acid residues of the MFE2 HD domain (Trp^{249}-Glu^{250}-Arg^{251}) as ligand adduct fragment (supplemental Fig. S1*A* and Fig. 6), and the MFE2 mutants bearing these residues (W249A, W249G, R251A) exhibited a decreased binding efficiency (Fig. 7). 3) Based on the three-dimensional structure of rat MFE2 HD, these residues are located apart from the catalytic center, but located on the tip of the hydrophobic cavity leading to the active site (Fig. 8). 4) The MFE2 mutants disrupting the aromatic and hydrophobic residues forming the hydrophobic cavity of the MFE2 HD domain (Y156S, I180N, I288N) were impaired in the interaction with the photoreactive LCFA probe (Fig. 9). The HD domain of MFE2 belongs to the short-chain alcohol dehydrogenase/reductase (SDR) super-

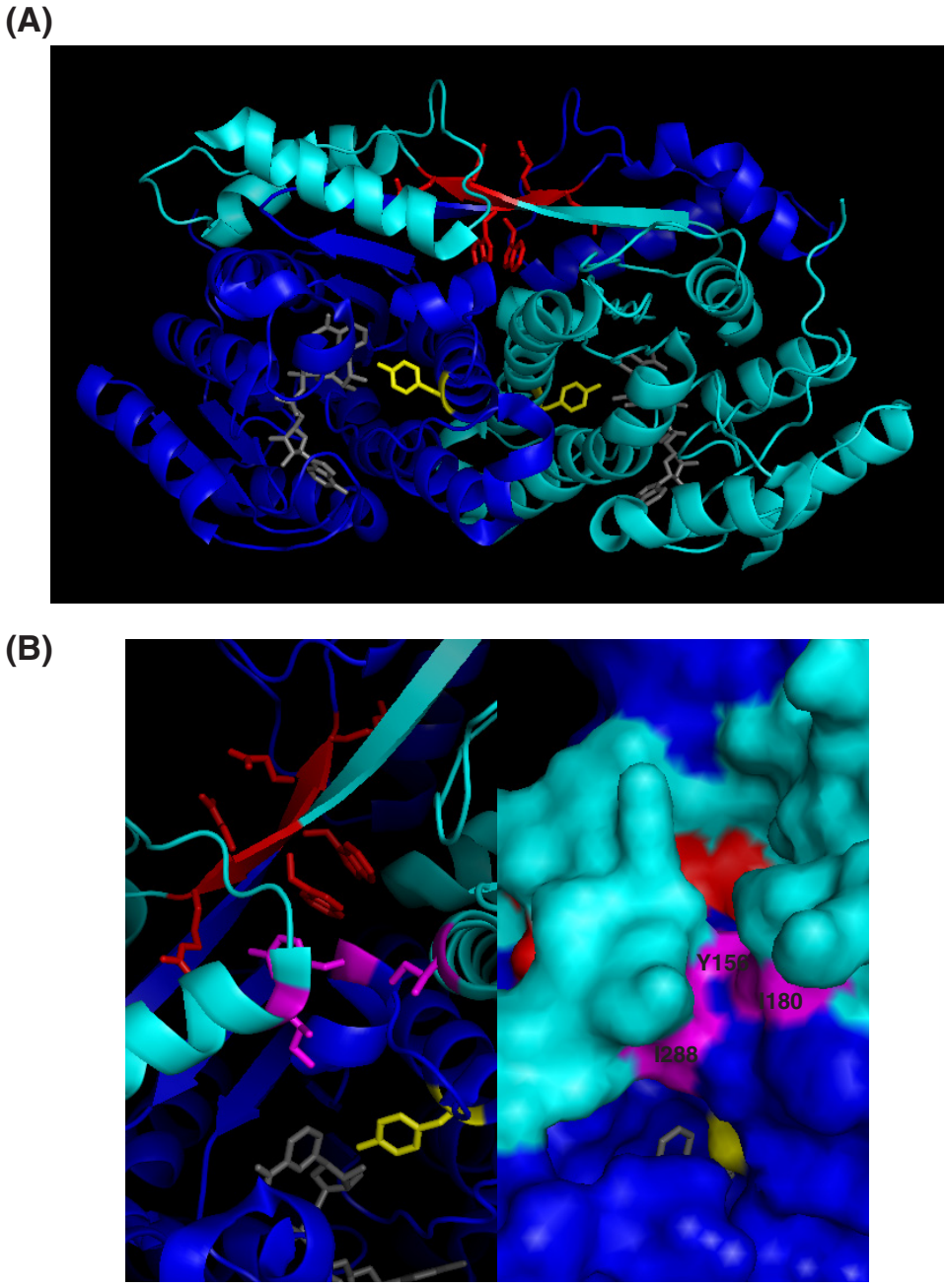

FIGURE 8. **Three-dimensional structure of MFE2 HD domain.** *A*, binary structure of rat MFE2HD (Protein Data Bank code 1GZ6). The structure consists of two identical monomers colored *blue* and *cyan*, respectively. The catalytic residue (Tyr^{164}) is colored *yellow*, and the probe-incorporated fragment (Trp^{249}-Arg^{251}) is colored *red*. The bound NAD^+ are shown as a stick model and colored *gray*. *B*, zoom-in view of the molecular surface of the putative substrate binding cavity. The catalytic residue (*Y164*) and the probe-incorporated fragment (*W249-R251*) are colored as described in *A*. Aromatic residue (*Y156*) and hydrophobic residues (*I160*, *I288*) forming the hydrophobic cavity are colored *magenta*. Images were generated using PyMOL.

family, containing a typical Rossmann-fold scaffold for NAD^+ binding and a Ser-Tyr-Lys triad for catalysis (47). The hydrophobic cavity leading to the active site also appears to be a common feature among members of the short-chain alcohol dehydrogenase/reductase family. Tanaka N. *et al.* (48) first reported a ternary structure of *E. coli* 7α-hydroxysteroid dehydrogenase, an short-chain alcohol dehydrogenase/reductase protein, complexed with NAD^+ and glycochenodeoxycholic acid as a substrate. Based on the ternary structure, the substrate was deposited in the hydrophobic cavity. In addition, 17β-estradiol and *R*-phenylethanol were shown to locate in the hydrophobic cavities of human 17β-hydroxysteroid dehydrogenase 1 and *Lactobacillus brevis R*-specific alcohol dehydrogenase, respectively (49, 50). These observations suggest that the hydrophobic cavity leading to the active site is important for substrate binding of short-chain alcohol dehydrogenase/reductase proteins. In the case of MFE2 HD, Ylianttila *et al.* (51) recently performed a docking study of 3*R*-hydroxydecanoyl-CoA to a heterodimer of yeast *Candida tropicalis* MFE2 HD-A and MFE2 HD-B. They hypothesized the residues of the COOH-terminal domain of MFE2 HD-B form hydrogen bonds with the phosphate groups of the CoA, and the fatty acid tail of the substrate could be guided into the hydrophobic pocket. Our studies also showed the diazirine photophore covalently attached to 3 amino acid residues in the COOH-terminal portion of MFE2 HD, and suggest that the fatty acid tail penetrates into the hydrophobic pocket of the other MFE2 HD (Fig. 9).

The three amino acid region (Trp^{249}-Glu^{250}-Arg^{251}), which we identified as a photoprobe anchoring site, is located on the dimer interface of the MFE2 HD domains. Among them, Trp^{249} of both monomers is positioned in close proximity and the side chains of the two tryptophan residues lie parallel with each other. Therefore, Trp^{249} is suggested to be important for homodimerization of the domains. Ferdinandusse *et al.* (38) identified a W249G mutation in a patient with MFE2 deficiency, and they considered the mutation to be responsible for dimerization based on structural analysis. In this study, MFE2(W249A) and MFE2(W249G) indeed affected the ligand binding efficiency (Fig. 7). However, these mutants as well wild type MFE2 exhibited a molecular mass corresponding to a dimer on sucrose density gradient centrifugation (data not shown). These data indicate that the tryptophan residue could be responsible for substrate binding and not solely for dimerization.

As for the photoaffinity studies on peroxisomal proteins, it was useful to identify the fatty acid-binding proteins. Mangroo *et al.* (52) previously found that acyl-CoA oxidase was

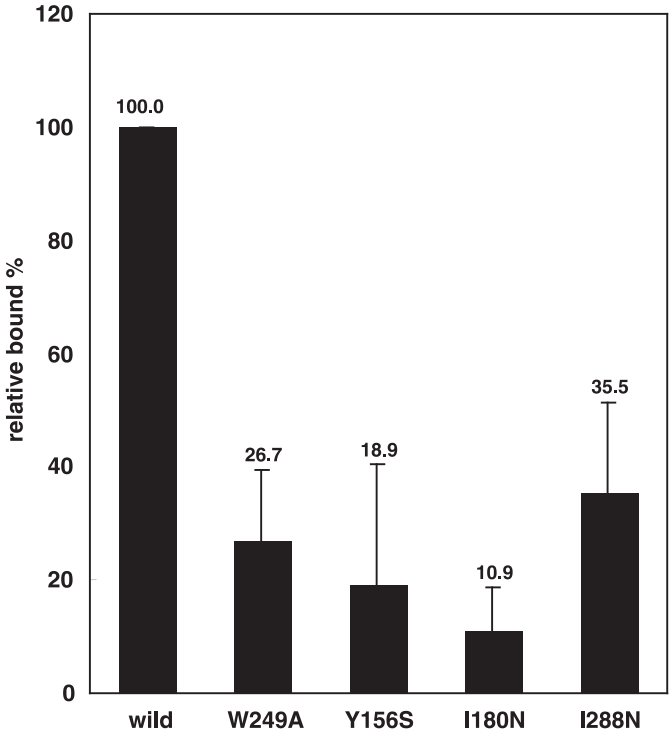

FIGURE 9. **Photoaffinity labeling of mutant MFE2-His.** Wild type and mutant MFE2-His (3.9 μg of protein) were photoaffinity labeled by the photoaffinity LCFA probe. The amount of probe-incorporated MFE2s was quantified with a LAS4000 luminoanalyzer and the relative labeling percentage was expressed as a ratio of the labeling percentage of each mutant MFE2 with that of wild type MFE2.

specifically labeled by 11-diazirinophenoxy-undecanoyl-CoA in the lysed peroxisomes of *C. tropicalis*. Rajasekharan *et al.* (53) reported that acyl-CoA oxidase was labeled *in vitro* with 12-azido-oleoyl-CoA and 12-(4-azidosalicyl)-aminododecanoyl-CoA. However, the precise mechanisms of their substrate binding were poorly understood.

In this study, we have identified a peroxisomal β-oxidation enzyme by photoaffinity labeling using a novel photoreactive LCFA probe. Furthermore, we aimed to develop a photochemical study to characterize the substrate binding mode of the protein. This technique would be useful to identify and characterize the fatty acid transporting proteins and metabolizing enzymes with some modifications.

Acknowledgments—We thank Dr. Shoji Okamura for excellent technical assistance on the MALDI-TOF analyses. We also thank Pacific Edit for assistance in editing the manuscript.

REFERENCES

1. Wanders, R. J., and Waterham, H. R. (2006) *Annu. Rev. Biochem.* **75,** 295–332
2. Lazarow, P. B., and Moser, H. W. (1995) *The Metabolic and Molecular Basis of Inherited Disease*, pp. 2287–2324, McGraw-Hill Inc., New York
3. Brosius, U., and Gärtner, J. (2002) *Cell. Mol. Life Sci.* **59,** 1058–1069
4. Fujiki, Y. (2000) *FEBS Lett.* **476,** 42–46
5. Wanders, R. J., and Waterham, H. R. (2006) *Biochim. Biophys. Acta* **1763,** 1707–1720
6. Wanders, R. J., Vreken, P., Ferdinandusse, S., Jansen, G. A., Waterham, H. R., van Roermund, C. W., and Van Grunsven, E. G. (2001) *Biochem. Soc. Trans.* **29,** 250–267
7. Osumi, T., Hashimoto, T., and Ui, N. (1980) *J. Biochem.* **87,** 1735–1746
8. Vanhove, G. F., Van Veldhoven, P. P., Fransen, M., Denis, S., Eyssen, H. J., Wanders, R. J., and Mannaerts, G. P. (1993) *J. Biol. Chem.* **268,** 10335–10344
9. Osumi, T., and Hashimoto, T. (1979) *Biochem. Biophys. Res. Commun.* **89,** 580–584
10. Furuta, S., Miyazawa, S., Osumi, T., Hashimoto, T., and Ui, N. (1980) *J. Biochem.* **88,** 1059–1070
11. Dieuaide-Noubhani, M., Novikov, D., Vandekerckhove, J., Veldhoven, P. P., and Mannaerts, G. P. (1997) *Biochem. J.* **321,** 253–259
12. Li, J. X., Smeland, T. E., and Schulz, H. (1990) *J. Biol. Chem.* **265,** 13629–13634
13. Jiang, L. L., Miyazawa, S., and Hashimoto, T. (1996) *J. Biochem.* **120,** 633–641
14. Qin, Y. M., Poutanen, M. H., Helander, H. M., Kvist, A. P., Siivari, K. M., Schmitz, W., Conzelmann, E., Hellman, U., and Hiltunen, J. K. (1997) *Biochem. J.* **321,** 21–28
15. Dieuaide-Noubhani, M., Novikov, D., Baumgart, E., Vanhooren, J. C., Fransen, M., Goethals, M., Vandekerckhove, J., Van Veldhoven, P. P., and Mannaerts, G. P. (1996) *Eur. J. Biochem.* **240,** 660–666
16. Dieuaide-Noubhani, M., Asselberghs, S., Mannaerts, G. P., and Van Veldhoven, P. P. (1997) *Biochem. J.* **325,** 367–373
17. Jiang, L. L., Kurosawa, T., Sato, M., Suzuki, Y., and Hashimoto, T. (1997) *J. Biochem.* **121,** 506–513
18. Novikov, D., Dieuaide-Noubhani, M., Vermeesch, J. R., Fournier, B., Mannaerts, G. P., and Van Veldhoven, P. P. (1997) *Biochim. Biophys. Acta* **1360,** 229–240
19. Qin, Y. M., Haapalainen, A. M., Conry, D., Cuebas, D. A., Hiltunen, J. K., and Novikov, D. K. (1997) *Biochem. J.* **328,** 377–382
20. Antonenkov, V. D., Van Veldhoven, P. P., Waelkens, E., and Mannaerts, G. P. (1997) *J. Biol. Chem.* **272,** 26023–26031
21. Kamijo, K., Taketani, S., Yokota, S., Osumi, T., and Hashimoto, T. (1990) *J. Biol. Chem.* **265,** 4534–4540
22. Kamijo, K., Kamijo, T., Ueno, I., Osumi, T., and Hashimoto, T. (1992) *Biochim. Biophys. Acta* **1129,** 323–327
23. Gärtner, J., Moser, H., and Valle, D. (1992) *Nat. Genet.* **1,** 16–23
24. Mosser, J., Douar, A. M., Sarde, C. O., Kioschis, P., Feil, R., Moser, H., Poustka, A. M., Mandel, J. L., and Aubourg, P. (1993) *Nature* **361,** 726–730
25. Lombard-Platet, G., Savary, S., Sarde, C. O., Mandel, J. L., and Chimini, G. (1996) *Proc. Natl. Acad. Sci. U.S.A.* **93,** 1265–1269
26. Holzinger, A., Kammerer, S., Berger, J., and Roscher, A. A. (1997) *Biochem. Biophys. Res. Commun.* **239,** 261–264
27. Moser, H. W., Moser, A. B., Frayer, K. K., Chen, W., Schulman, J. D., O'Neill, B. P., and Kishimoto, Y. (1981) *Neurology* **31,** 1241–1249
28. Moser, H. W., Moser, A. B., Kawamura, N., Murphy, J., Suzuki, K., Schaumburg, H., and Kishimoto, Y. (1980) *Ann. Neurol.* **7,** 542–549
29. Imanaka, T., Aihara, K., Takano, T., Yamashita, A., Sato, R., Suzuki, Y., Yokota, S., and Osumi, T. (1999) *J. Biol. Chem.* **274,** 11968–11976
30. Imanaka, T., Shiina, Y., Takano, T., Hashimoto, T., and Osumi, T. (1996) *J. Biol. Chem.* **271,** 3706–3713
31. Corey, E. J., Xu, F., and Noe, M. C. (1997) *J. Am. Chem. Soc.* **119,** 12414–12415
32. Hashimoto, M., Hatanaka, Y., Sadakane, Y., and Nabeta, K. (2002) *Bioorg. Med. Chem. Lett.* **12,** 2507–2510
33. de Duve, C., Pressman, B. C., Gianetto, R., Wattiaux, R., and Appelmans, F. (1955) *Biochem. J.* **60,** 604–617
34. Haapalainen, A. M., Koski, M. K., Qin, Y. M., Hiltunen, J. K., and Glumoff, T. (2003) *Structure* **11,** 87–97
35. Nakashima, H., Hashimoto, M., Sadakane, Y., Tomohiro, T., and Hatanaka, Y. (2006) *J. Am. Chem. Soc.* **128,** 15092–15093
36. Huyghe, S., Mannaerts, G. P., Baes, M., and Van Veldhoven, P. P. (2006) *Biochim. Biophys. Acta* **1761,** 973–994
37. Kashiwayama, Y., Asahina, K., Shibata, H., Morita, M., Muntau, A. C., Roscher, A. A., Wanders, R. J., Shimozawa, N., Sakaguchi, M., Kato, H., and Imanaka, T. (2005) *Biochim. Biophys. Acta* **1746,** 116–128
38. Ferdinandusse, S., Ylianttila, M. S., Gloerich, J., Koski, M. K., Oostheim, W., Waterham, H. R., Hiltunen, J. K., Wanders, R. J., and Glumoff, T. (2006) *Am. J. Hum. Genet.* **78,** 112–124

39. Watkins, P. A., Chen, W. W., Harris, C. J., Hoefler, G., Hoefler, S., Blake, D. C., Jr., Balfe, A., Kelley, R. I., Moser, A. B., and Beard, M. E. (1989) *J. Clin. Invest.* **83,** 771–777
40. Suzuki, Y., Jiang, L. L., Souri, M., Miyazawa, S., Fukuda, S., Zhang, Z., Une, M., Shimozawa, N., Kondo, N., Orii, T., and Hashimoto, T. (1997) *Am. J. Hum. Genet.* **61,** 1153–41162
41. Van Grunsven, E. G., van Berkel, E., Ijlst, L., Vreken, P., de Klerk, J. B., Adamski, J., Lemonde, H., Clayton, P. T., Cuebas, D. A., and Wanders, R. J. (1998) *Proc. Natl. Acad. Sci. U.S.A.* **95,** 2128–2133
42. Van Grunsven, E. G., van Berkel, E., Mooijer, P. A., Watkins, P. A., Moser, H. W., Suzuki, Y., Jiang, L. L., Hashimoto, T., Hoefler, G., Adamski, J., and Wanders, R. J. (1999) *Am. J. Hum. Genet.* **64,** 99–107
43. Baes, M., Huyghe, S., Carmeliet, P., Declercq, P. E., Collen, D., Mannaerts, G. P., and Van Veldhoven, P. P. (2000) *J. Biol. Chem.* **275,** 16329–16336
44. Jiang, L. L., Kobayashi, A., Matsuura, H., Fukushima, H., and Hashimoto, T. (1996) *J. Biochem.* **120,** 624–632
45. Leenders, F., Tesdorpf, J. G., Markus, M., Engel, T., Seedorf, U., and Adamski, J. (1996) *J. Biol. Chem.* **271,** 5438–5442
46. Adamski, J., Leenders, F., Carstensen, J. F., Kaufmann, M., Markus, M. M., Husen, B., Tesdorpf, J. G., Seedorf, U., de Launoit, Y., and Jakob, F. (1997) *Steroids* **62,** 159–163
47. Filling, C., Berndt, K. D., Benach, J., Knapp, S., Prozorovski, T., Nordling, E., Ladenstein, R., Jörnvall, H., and Oppermann, U. (2002) *J. Biol. Chem.* **277,** 25677–25684
48. Tanaka, N., Nonaka, T., Tanabe, T., Yoshimoto, T., Tsuru, D., and Mitsui, Y. (1996) *Biochemistry* **35,** 7715–7730
49. Breton, R., Housset, D., Mazza, C., and Fontecilla-Camps, J. C. (1996) *Structure* **4,** 905–915
50. Schlieben, N. H., Niefind, K., Müller, J., Riebel, B., Hummel, W., and Schomburg, D. (2005) *J. Mol. Biol.* **349,** 801–813
51. Ylianttila, M. S., Pursiainen, N. V., Haapalainen, A. M., Juffer, A. H., Poirier, Y., Hiltunen, J. K., and Glumoff, T. (2006) *J. Mol. Biol.* **358,** 1286–1295
52. Mangroo, D., Steele, L., Rachubinski, R. A., and Gerber, G. E. (1993) *Biochim. Biophys. Acta* **1168,** 280–284
53. Rajasekharan, R., Marians, R. C., Shockey, J. M., and Kemp, J. D. (1993) *Biochemistry* **32,** 12386–12391